Identifying the Driver of Pulsating Aurora

Y. Nishimura *et al.*

Science **330**, 81 (2010);
DOI: 10.1126/science.1193186

Our data show that people occupied a New Guinea valley at 2000 m above sea level soon after their arrival in Sahul (*1*). As the climate cooled, the optimal growing conditions for yams would have occurred at lower altitudes. This may indicate that *Pandanus* was the most important staple at this time and help explain the late Pleistocene abandonment of the highland sites. Foraging into this high-altitude environment would guarantee a high return in plant fat and protein to complement local animal foods, the starch-rich yams from lower altitudes, and those foods not preserved in the archaeological record.

References and Notes

1. J. F. O'Connell, J. Allen, *J. Archaeol. Sci.* **31**, 835 (2004).
2. J. P. White *et al.*, *Proc. Prehistoric Soc.* **36**, 152 (1970).
3. A. Fairbairn, G. Hope, G. Summerhayes, *World Archaeol.* **38**, 371 (2006).
4. P. J. Reimer *et al.*, *Radiocarbon* **51**, 1111 (2010).
5. I. Farrera *et al.*, *Clim. Dyn.* **15**, 823 (1999).
6. G. Hope, *Quat. Sci. Rev.* **28**, 2261 (2009).
7. A. L. Daniau *et al.*, *Quat. Sci. Rev.*, 10.1016/j.quascirev.2009.11.008 (2009).
8. L. Groube, in *Foraging and Farming: The Evolution of Plant Exploitation*, D. R. Harris, G. C. H. Hillman, Eds. (Unwin, London, 1989), pp. 292–304.
9. L. Groube, J. Chappell, J. Muke, D. Price, *Nature* **324**, 453 (1986).
10. B. C. Stone, *Econ. Bot.* **38**, 304 (1984).
11. M. J. Mountain, in *Man and a Half: Essays in Pacific Anthropology and Ethnobiology in Honour of Ralph Bulmer*, A. Pawley, Ed. (Polynesian Society, Auckland, New Zealand, 1991), pp. 510–520.

12. This research was supported by the Marsden Fund Council from government funding administered by the Royal Society of New Zealand. We thank G. Hope for introducing us to the Ivane Valley and companionship in the field; the communities of the Ivane Valley for their support; and the National Research Institute of PNG and the National Museum and Art Gallery of PNG for their support and affiliation. The authors acknowledge the facilities as well as scientific and technical assistance from the staff at the Australian Microscopy and Microanalysis Research Facility and the Australian Centre for Microscopy and Microanalysis at the University of Sydney. We thank L. O'Neill and M. Hennessey for the illustrations and J. Allen and M. Weisler for providing comments on a draft of the paper. J.F. thanks R. Torrence for access to the Australian Museum PNG starch reference collection. R.F. is indebted to the Australian Museum and the University of Sydney for facilitating the import of quarantined material and access to laboratory space.

Supporting Online Material

www.sciencemag.org/cgi/content/full/330/6000/78/DC1
SOM Text
Figs. S1 to S9
Tables S1 to S3
References

2 June 2010; accepted 23 July 2010
10.1126/science.1193130

Identifying the Driver of Pulsating Aurora

Y. Nishimura,[1,2*] J. Bortnik,[1] W. Li,[1] R. M. Thorne,[1] L. R. Lyons,[1] V. Angelopoulos,[3,4,5] S. B. Mende,[4] J. W. Bonnell,[4] O. Le Contel,[6] C. Cully,[7] R. Ergun,[8] U. Auster[9]

Pulsating aurora, a spectacular emission that appears as blinking of the upper atmosphere in the polar regions, is known to be excited by modulated, downward-streaming electrons. Despite its distinctive feature, identifying the driver of the electron precipitation has been a long-standing problem. Using coordinated satellite and ground-based all-sky imager observations from the THEMIS mission, we provide direct evidence that a naturally occurring electromagnetic wave, lower-band chorus, can drive pulsating aurora. Because the waves at a given equatorial location in space correlate with a single pulsating auroral patch in the upper atmosphere, our findings can also be used to constrain magnetic field models with much higher accuracy than has previously been possible.

The aurora is a spectacular natural phenomenon that occurs in Earth's polar regions, exhibiting a range of scale sizes (~1 to 100 km) and characteristic wavelengths (e.g., 427.8, 557.7, and 630.0 nm) (*1*, *2*). Auroral features are a visual display of the patterns of energetic particles from distant regions in Earth's magnetosphere that move along magnetic field lines, causing photon emissions in the upper atmosphere. This process represents an important loss of energetic particles from the magnetosphere, and the energy from these particles causes drastic changes in ionization of the upper atmosphere. One type of aurora, the pulsating aurora (PA), has attracted much attention because of its distinctive luminosity patches at ~100-km altitude, which have a horizontal scale size of ~100 km and switch on and off with recurrence periods of ~5 to 40 s (*3*, *4*).

Rocket and low-altitude spacecraft observations have revealed that auroral pulsations result from a time-varying flux of precipitating electrons with energies exceeding ~10 keV (*3*, *5*). However, the driver of this precipitation has not been uniquely identified. Theoretical investigations have shown that resonant interactions with naturally occurring emissions, known as chorus, could lead to the precipitation of energetic electrons in the appropriate energy range for PA (*4*, *6*), but this suggestion has been difficult to verify experimentally. Chorus consists of discrete bursts of wave power that are confined near the magnetic equator (*7*, *8*) and typically occur in distinct lower- and upper-frequency bands, below and above half of the equatorial electron cyclotron frequency (f_c). Lower- and upper-band chorus can resonate with more than 10 and less than a few keV electrons (*9*), respectively. In addition, chorus may evolve nonlinearly for large amplitudes (*10*) and is frequently associated with electrostatic cyclotron harmonic (ECH) waves, which occur above 1 f_c and can resonate with electrons of energies below a few keV (*11*).

Attempts have been made to test wave theories using low-altitude rocket observations (*12*) and high-altitude, equatorial spacecraft (*13*–*15*). Although a general correspondence between PA and electromagnetic waves has been observed, a one-to-one correlation between individual bursts of chorus and auroral pulses has been elusive. This discrepancy between observation and theoretical prediction has been attributed to the difficulty in finding the exact mapping of a distant spacecraft to a small (~100 km) pulsating auroral patch in the upper atmosphere along magnetic field lines. Such mapping is particularly difficult because adjacent auroral patches typically pulsate independently of each other (*16*). Additionally, the simultaneous existence of multiple magnetospheric plasma waves (*13*, *17*) makes it difficult to identify the specific wave mode responsible for electron scattering leading to PA.

Here, we report observations of PA obtained on 15 February 2009 using one of the ground-based All-Sky Imagers (ASIs) (*18*) of the THEMIS mission (*19*). Their broad latitudinal and longitudinal coverage (~1000 km), as well as high resolution (~1 km spatial and 3 s temporal), allowed us to observe the evolution of localized, individual pulsating auroral patches. We also report on plasma wave observations made in space by THEMIS-A (*20*–*22*). During the period of observation, this spacecraft was located near the magnetic equator in the Southern Hemisphere, and the magnetic field line threading the spacecraft was located close to the center of the imager field of view, which avoids optical distortion.

In the model shown in Fig. 1A, electrons that are initially trapped by Earth's magnetic field encounter chorus propagating away from the equator. The electrons are scattered and precipitate into the upper atmosphere, resulting in

[1]Department of Atmospheric and Oceanic Sciences, University of California, Los Angeles, CA 90095, USA. [2]Solar-Terrestrial Environment Laboratory, Nagoya University, Nagoya, Aichi 464-8601, Japan. [3]Institute of Geophysics and Planetary Physics, University of California, Los Angeles, CA 90095, USA. [4]Space Sciences Laboratory, University of California, Berkeley, CA 94720–7450, USA. [5]Jet Propulsion Laboratory. National Aeronautics and Space Administration, Pasadena, CA 91109, USA. [6]Laboratoire de Physique des Plasmas, CNRS/Ecole Polytechnique/UPMC/Paris-Sud 11, F-94107 St Maur-des-Fossés, France. [7]Swedish Institute of Space Physics, SE-981 28 Uppsala, Sweden. [8]Laboratory for Atmospheric and Space Physics, University of Colorado, Boulder, CO 80303–7814, USA. [9]Institut für Geophysik und extraterrestrische Physik, Technischen Universität Braunschweig, Braunschweig D-38106, Germany.

*To whom correspondence should be addressed. E-mail: toshi@atmos.ucla.edu

the auroral light observed by the ASI. A typical lower-band chorus spectrum at frequencies between 0.05 and 0.3 f_c (Fig. 1B) shows repetitive discrete bursts every ~10 s, which would be composed of multiple chorus elements. Intense lower-band chorus was present during this time period, whereas both upper-band chorus (0.5 to 0.8 f_c) and ECH (>1.0 f_c) waves were not observed, even though the spacecraft was located close to the equator.

Images from the Narsarsuaq (Greenland) ASI (Fig. 1C) at the four selected times (see movie S1 for the entire image sequence) display discrete aurora, which is the bright, structured emission in the northern portion, as well as fainter, unstructured emissions to the south, called diffuse aurora. Auroral patches with a scale size of ~100 km pulsating at ~64° to 67° magnetic latitude (MLAT) embedded in the diffuse aurora are PA; their repetitive intensity modulation is seen clearly in movie S1. The images in the second and fourth panels in Fig. 1C were obtained simultaneously with intense chorus shown in Fig. 1B (vertical lines b and d). A bright auroral patch to the west of the model footprint of the spacecraft is not present in the first and third panels. Adjacent auroral patches do not pulsate in phase with the chorus intensity modulation, implying a correlation between the chorus emission measured at the spacecraft and the pulsating auroral patch. It is thus likely that the auroral patch that best correlates with the chorus intensity modulation pinpoints the source of the precipitation in space and the correct footprint of the spacecraft rather than the model footprint shown in Fig. 1C.

To investigate this hypothesis, we calculated cross-correlation coefficients between the lower-band chorus intensity and auroral luminosity in each imager pixel using the entire period of the wave observations shown in Fig. 1B. The auroral pulsations have an almost one-to-one correspondence with each burst of chorus (Fig. 1D). The high correlation (0.88, SE = 0.13) supports our inference that intensity-modulated lower-band chorus was driving this PA. Although the time lag between these two wave forms was considered, we found that the simultaneous correlation was much higher. This is consistent with the short travel times (<1 s) of >10 keV precipitating equatorial electrons down the field line causing PA, and the short lifetime (~1 s) of the excited atmospheric atoms (*23*). Both of these time scales fall within the time resolution of the imager (3 s).

We also calculated spatial distributions of the cross-correlation coefficient for all imager pixels. The first image of Fig. 2B reveals a well-grouped patch of high correlation. The correlation coefficient outside this patch diminishes rapidly with distance, despite the presence of several other pulsating auroral patches located within the imager field of view. The high-correlation region demarcates the auroral patch marked in panels b and d of Fig. 1C, highlighting that this is the only

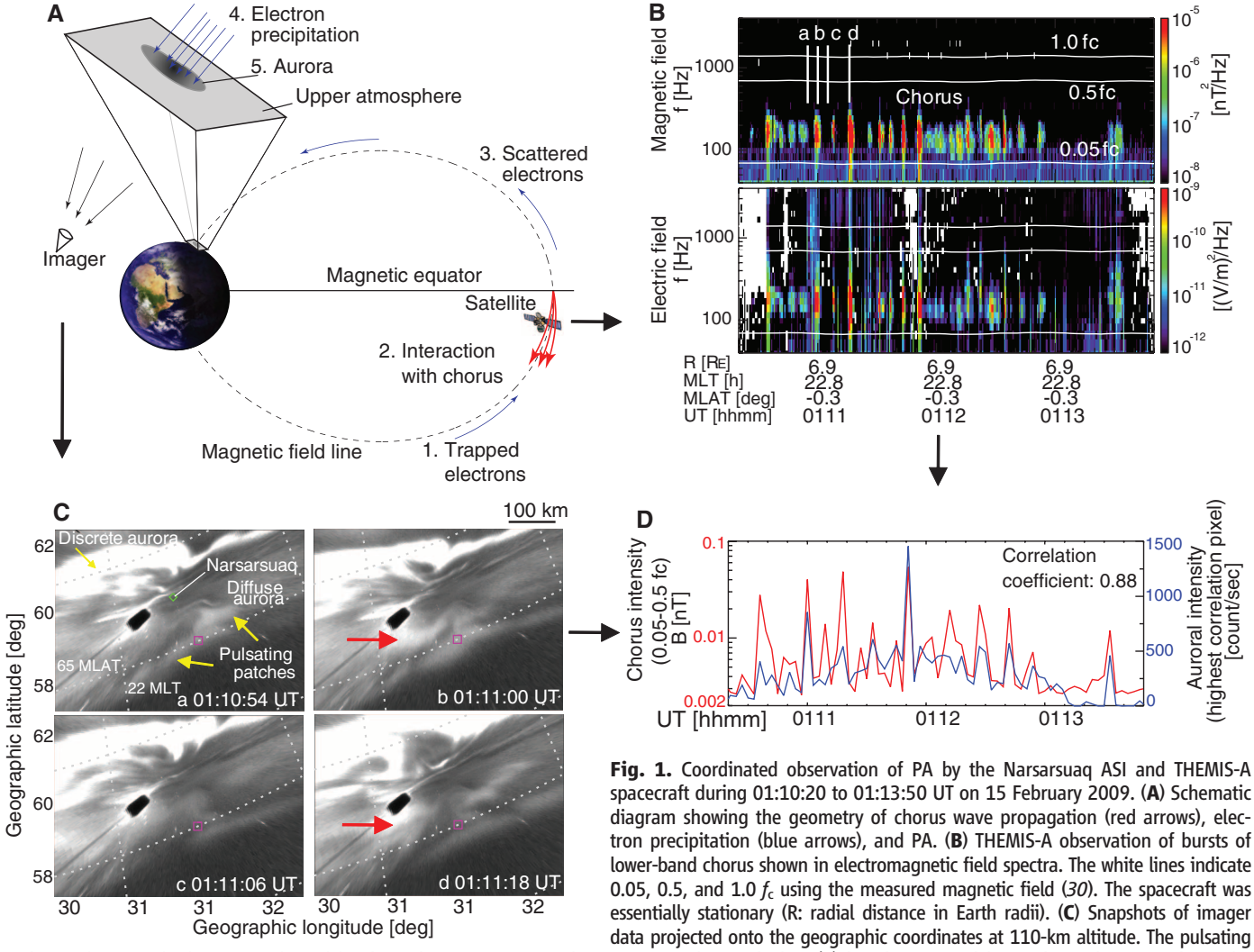

Fig. 1. Coordinated observation of PA by the Narsarsuaq ASI and THEMIS-A spacecraft during 01:10:20 to 01:13:50 UT on 15 February 2009. (**A**) Schematic diagram showing the geometry of chorus wave propagation (red arrows), electron precipitation (blue arrows), and PA. (**B**) THEMIS-A observation of bursts of lower-band chorus shown in electromagnetic field spectra. The white lines indicate 0.05, 0.5, and 1.0 f_c using the measured magnetic field (*30*). The spacecraft was essentially stationary (R: radial distance in Earth radii). (**C**) Snapshots of imager data projected onto the geographic coordinates at 110-km altitude. The pulsating patch correlating with chorus is indicated by the red arrows. ASI snapshot times are also marked in (B) by white vertical lines. The pink square shows the magnetic footprint of the THEMIS-A spacecraft using the Tsyganenko 96 (*31*) magnetic field model (the model was used only for a rough estimation of the footprint, and the choice of the model is arbitrary). The spacecraft footprint was located close to the center of the imager field of view (green square in panel a). Dashed lines give magnetic coordinates every 3° in latitude and 1 hour in local time. The black spot near the center of each image is an artificial object. (**D**) Correlation of lower-band chorus integrated magnetic field intensity over 0.05 to 0.5 f_c (red) and auroral intensity (blue) at the highest cross-correlation pixel.

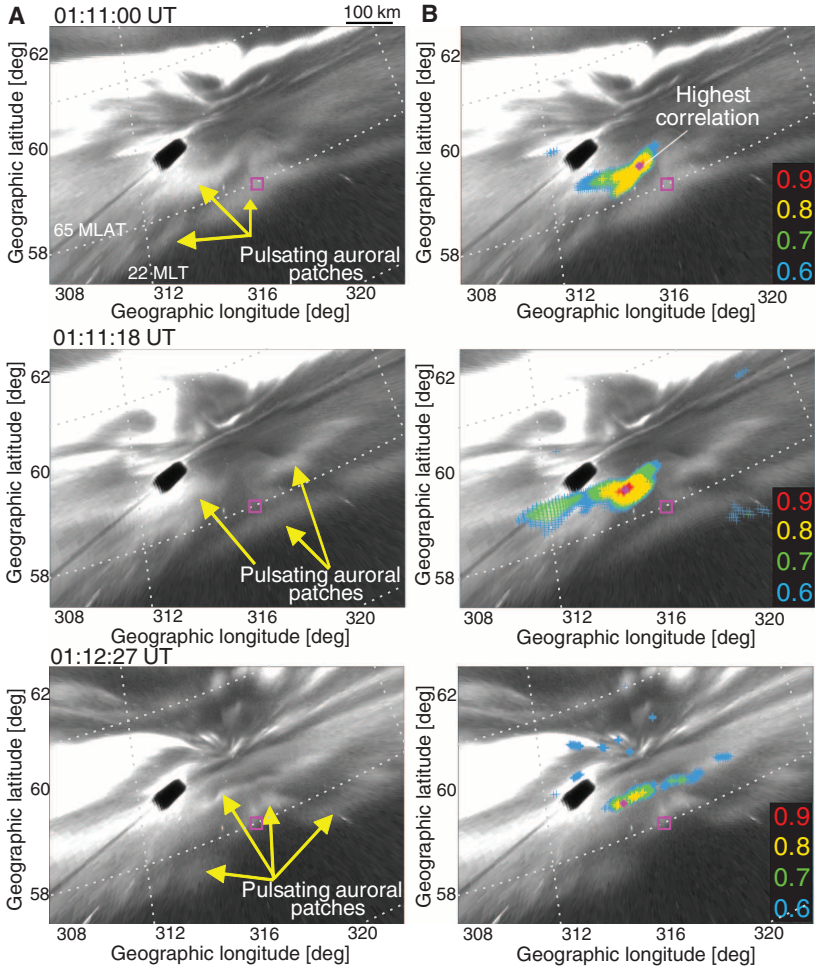

Fig. 2. Spatial distribution of the aurora-chorus cross-correlation during the observations of Fig. 1. (**A**) PA and (**B**) cross-correlation coefficient superimposed onto the images during the 1-min time interval, including each snapshot time in (A). Pixels with correlation coefficient below 0.6 are not color-coded. The image format is the same as in Fig. 1C.

auroral patch that is correlated with the chorus intensity variation. The highest cross-correlation (0.91) is located 0.83° MLAT north and 0.07 hour in magnetic local time (MLT) (80 km) west of the model footprint.

The cross-correlation coefficients calculated for the later images (second and third rows in Fig. 2B) are spatially grouped on a pulsating patch as in the top row, again indicating that only a single pulsating patch is correlated with the chorus intensity. While the patch shape changes with time, the location of highest correlation stays essentially fixed, providing further support for the association of the PA to wave-induced precipitation originating at the spacecraft location.

The dominant role of lower-band chorus in driving the PA is further illustrated in Fig. 3 in different times (*24*). During the longer-duration chorus event (Fig. 3A and movie S2), the time series of the wave intensity and auroral luminosity were again in close agreement (the correlation coefficient is 0.71), indicating that the duration of each occurrence of PA is controlled by the modulation of lower-band chorus (*25*).

For the event shown in Fig. 3B measured in another time period, lower-band chorus was negligible but intense ECH waves were present. As shown in movie S1, diffuse aurora without pulsations extended over a wide latitudinal range near the longitude of the spacecraft after 01:15 UT. The cross-correlation analysis found the diffuse aurora region as having the highest correlation (0.73) with the ECH waves. A comparison of the time series (Fig. 3B, bottom panel) captures the simultaneous auroral intensification and the pronounced enhancement of ECH intensity. The aurora, however, did not pulsate but stayed at a high intensity after the initial increase, indicating that ECH waves can indeed (*11*) contribute

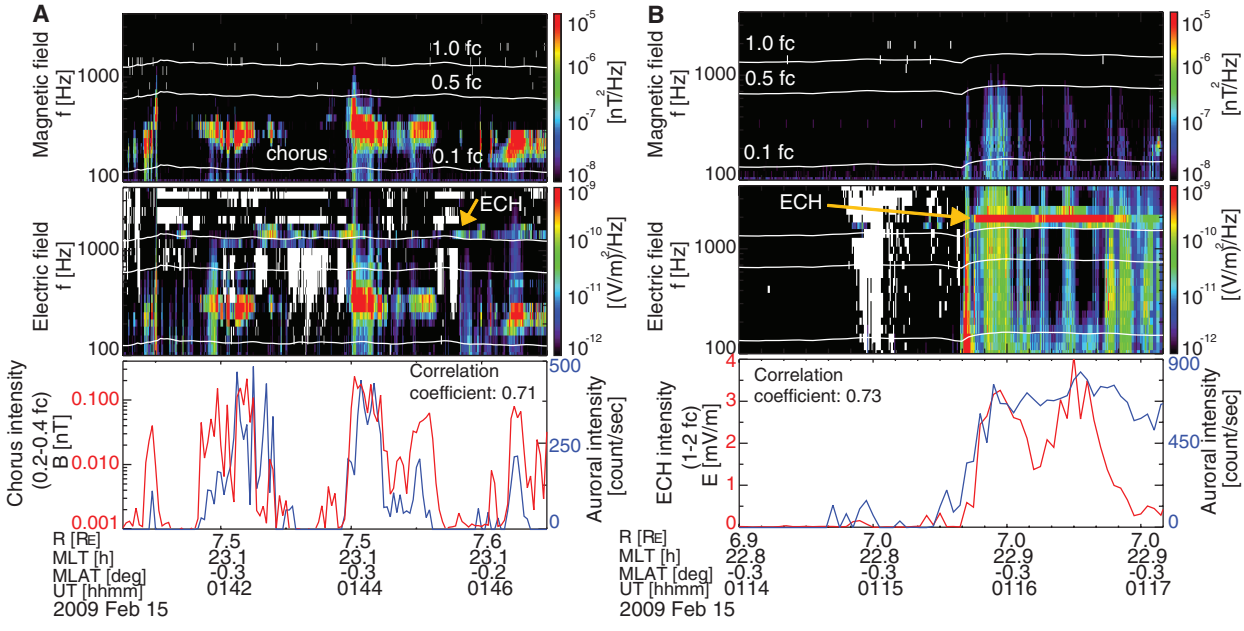

Fig. 3. THEMIS-A–imager correlation analysis results during (**A**) longer-duration chorus and (**B**) ECH events. The format is the same as in Fig. 1, B and D. The entire auroral sequences are given in movie S2 and the latter part of movie S1.

to the diffuse aurora but are not responsible for the pulsating patches (*26*).

Theoretical calculations (*9*, *27*) using the observed lower-band chorus amplitudes (~50 pT) show that such amplitudes are sufficiently strong to cause precipitation of ~10-keV electrons into the atmosphere. Wave burst observations with higher resolution (fig. S1) indicate more intense fields (~30 mV/m and ~1 nT) that were quasi–field-aligned and propagated away from the equator, making the interaction with electrons that precipitate into the atmosphere and drive PA substantially more efficient near the equator (less than ~15°) because of Landau damping and increasing resonant energy in latitude. Each chorus element generated near the equator with a characteristic size of ~100 to 3000 km (*7*, *28*) and the oblique propagation away from the original magnetic field line (*10*, *29*) would lead to interaction regions with a typical patch size (~100 km in the ionosphere and ~a few thousand km in the magnetosphere).

Magnetic field line mapping has been a problematic issue in magnetosphere-ionosphere coupling studies. Based on the property that the high-correlation region occurs over a single auroral patch with the correlation coefficient outside this area diminishing quickly with distance, PA can be used to highlight the physical link between chorus wave activity and each auroral pulsation. The PA thus provides a unique opportunity to identify the footprint of the magnetic field line threading the spacecraft, to a precision within the auroral patch size (less than ~100 km) and possibly even down to a few imager pixels (~km).

References and Notes

1. T. Yamamoto, *J. Geophys. Res.* **93** (A2), 897 (1988).
2. D. McEwen *et al.*, *Can. J. Phys.* **59**, 1106 (1981).
3. A. Johnstone, *Nature* **274**, 119 (1978).
4. G. Davidson, *Space Sci. Rev.* **53**, 45 (1990).
5. I. Sandahl, L. Eliasson, R. Lundin, *Geophys. Res. Lett.* **7**, 309 (1980).
6. F. Coroniti, C. Kennel, *J. Geophys. Res.* **75**, 1863 (1970).
7. O. Santólik, D. A. Gurnett, J. S. Pickett, *Ann. Geophys.* **22**, 2555 (2004).
8. N. Meredith, R. B. Horne, R. M. Thorne, R. R. Anderson, *Geophys. Res. Lett.* **30**, 1871 (2003).
9. B. Ni, R. M. Thorne, Y. Y. Shprits, J. Bortnik, *Geophys. Res. Lett.* **35**, L11106 (2008).
10. J. Bortnik, R. M. Thorne, U. S. Inan, *Geophys. Res. Lett.* **35**, L21102 (2008).
11. R. Horne, R. M. Thorne, N. P. Meredith, R. R. Anderson, *J. Geophys. Res.* **108**, 1290 (2003).
12. D. Bryant *et al.*, *J. Atmos. Terr. Phys.* **33**, 859 (1971).
13. M. Gough *et al.*, *Adv. Space Res.* **1**, 345 (1981).
14. I. Ward, M. Lester, R. Thomas, *J. Atmos. Terr. Phys.* **44**, 931 (1982).
15. A. Johnstone, *Ann. Geophys.* **1**, 397 (1983).
16. M. Scourfield, W. Innes, N. Parsons, *Planet. Space Sci.* **20**, 1843 (1972).
17. J. Liang *et al.*, *J. Geophys. Res.* 10.1029/2009JA015148 (2010).
18. S. Mende *et al.*, *Space Sci. Rev.* **141**, 357 (2008).
19. V. Angelopoulos, *Space Sci. Rev.* **141**, 5 (2008).
20. J. Bonnell *et al.*, *Space Sci. Rev.* **141**, 303 (2008).
21. O. Le Contel *et al.*, *Space Sci. Rev.* **141**, 509 (2008).
22. C. Cully, R. E. Ergun, K. Stevens, A. Nammari, J. Westfall, *Space Sci. Rev.* **141**, 343 (2008).
23. A. Brekke, K. Henriksen, *Planet. Space Sci.* **20**, 53 (1972).
24. We also analyzed other events (table S1).
25. Weak ECH waves that may lead to weak auroral emission were also observed in the electric field spectra above 1.0 f_c.
26. The auroral intensity did not diminish following the decrease in the ECH intensity but stayed at a high level. This is attributable to the long lifetime (~1 min) of excited oxygen atom at higher altitudes (*32*) due to the precipitation of lower-energy electrons (~1 keV), as expected from resonance with ECH (*11*).
27. W. Li, Y. Y. Shprits, R. M. Thorne, *J. Geophys. Res.* **112**, A10220 (2007).
28. O. Agapitov *et al.*, *Ann. Geophys.* **28**, 1377 (2010).
29. W. Li *et al.*, *J. Geophys. Res.* **114**, A00C14 (2009).
30. H. Auster *et al.*, *Space Sci. Rev.* **141**, 135 (2008).
31. N. Tsyganenko, D. Stern, *J. Geophys. Res.* **101** (A12), 27187 (1996).
32. A. Omholt, *Planet. Space Sci.* **2**, 246 (1960).

33. This work was supported by NASA contract NAS5-02099, 9F007-046101; NSF grants ATM-0802843 and AGS-0840178; and a Research Fellowship from the Japan Society for the Promotion of Science. The French involvement (Search-coil magnetometer) on THEMIS is supported by CNES and CNRS.

Supporting Online Material

www.sciencemag.org/cgi/content/full/330/6000/81/DC1
Fig. S1
Table S1
Movies S1 and S2

3 June 2010; accepted 19 August 2010
10.1126/science.1193186

Cellodextrin Transport in Yeast for Improved Biofuel Production

Jonathan M. Galazka,[1] Chaoguang Tian,[2,3] William T. Beeson,[4] Bruno Martinez,[5] N. Louise Glass,[2] Jamie H. D. Cate[1,4,5]*

Fungal degradation of plant biomass may provide insights for improving cellulosic biofuel production. We show that the model cellulolytic fungus *Neurospora crassa* relies on a high-affinity cellodextrin transport system for rapid growth on cellulose. Reconstitution of the *N. crassa* cellodextrin transport system in *Saccharomyces cerevisiae* promotes efficient growth of this yeast on cellodextrins. In simultaneous saccharification and fermentation experiments, the engineered yeast strains more rapidly convert cellulose to ethanol when compared with yeast lacking this system.

The bioethanol industry uses the yeast *Saccharomyces cerevisiae* to ferment sugars derived from cornstarch or sugarcane into ethanol (*1*). Plant cell walls provide an abundant alternate sugar source yet remain largely unused (*2*, *3*). Present strategies for using plant biomass use large quantities of cellulase cocktails to release glucose from plant cell walls, posing economic and logistical challenges for implementation of these processes (*4*). Furthermore, *S. cerevisiae* cannot ferment the cellodextrins naturally released by cellulases (*5*, *6*) and require cellulase cocktails supplemented by β-glucosidases to quantitatively produce fermentable glucose (*7*).

In contrast to *S. cerevisiae*, cellulolytic fungi grow well on cellodextrins. The model cellulolytic fungus *Neurospora crassa*, when grown on pure cellulose, increases transcription of seven major facilitator superfamily (MFS) sugar transporters as well as an intracellular β-glucosidase (*8*). A strain carrying a deletion for one of these predicted transporters, NCU08114, grew slowly on cellulose (fig. S1) (*9*), and strains lacking either NCU08114 or NCU00801 poorly consumed cellobiose, cellotriose, and cellotetraose (fig. S2). Orthologs of NCU08114 and NCU00801 are widely distributed in the fungal kingdom (Fig. 1A) (*10*–*13*), and recent whole-genome transcriptional profiling studies show their importance to interactions between fungi and plants. For example, some cellulolytic fungi increase expression levels of NCU08114 orthologs while degrading plant wall material (*10*), and the Périgord black truffle increases the expression of a NCU00801 ortholog during symbiotic interactions with plant roots (*11*). In addition, certain yeasts that grow on cellobiose contain orthologs of NCU08114 and NCU00801 (*12*). All of these organisms also contain genes for intracellular β-glucosidases (*10*), suggesting that cellodextrin transport systems are widespread in nature and are essential for optimal growth of fungi on cellulose-derived sugars.

Because cellobiose is not catabolized by *S. cerevisiae* (*5*, *6*) and is not accumulated in the cytoplasm (fig. S3), we reasoned that expression of a functional cellodextrin transport system from *N. crassa* might allow *S. cerevisiae* to grow with cellobiose as the sole carbon source. Yeast strains expressing NCU00801 or NCU08114, together with the intracellular β-glucosidase NCU00130 (hereafter named GH1-1), grew on cellobiose at rates of about 30 and 12% of the rate of *S. cerevisiae* on glucose, respectively (Fig. 1B and fig. S4). Cellodextrins longer than cellobiose also support the growth of yeast expressing these transporters (Fig. 1C), indicating that cellodextrins longer than cellobiose are transported by NCU00801 and NCU08114, hereafter called CDT-1 and CDT-2,

[1]Department of Molecular and Cell Biology, University of California at Berkeley, Berkeley, CA 94720, USA. [2]Department of Plant and Microbial Biology, University of California at Berkeley, Berkeley, CA 94720, USA. [3]Tianjin Institute of Industrial Biotechnology, Chinese Academy of Sciences, Xiqi Dao 32, Tianjin Airport Economic Area, Tianjin 300308, China. [4]Department of Chemistry, University of California at Berkeley, Berkeley, CA 94720, USA. [5]Physical Biosciences Division, Lawrence Berkeley National Laboratory, Berkeley, CA 94720, USA.

*To whom correspondence should be addressed. E-mail: jcate@lbl.gov